

***SIFThinker*: Spatially-Aware Image Focus for Visual Reasoning**

**Zhangquan Chen^{1*}, Ruihui Zhao², Chuwei Luo², Mingze Sun¹, Xinlei Yu³,
Yangyang Kang^{2†}, Ruqi Huang^{1†}**

¹Tsinghua Shenzhen International Graduate School, Tsinghua University, China

²ByteDance, China

³National University of Singapore, Singapore

Abstract

Current multimodal large language models (MLLMs) still face significant challenges in complex visual tasks (e.g., spatial understanding, fine-grained perception). Prior methods have tried to incorporate visual reasoning, however, they fail to leverage attention correction with spatial cues to iteratively refine their focus on prompt-relevant regions. In this paper, we introduce *SIFThinker*, a spatially-aware “think-with-images” framework that mimics human visual perception. Specifically, *SIFThinker* enables attention correcting and image region focusing by interleaving depth-enhanced bounding boxes and natural language. Our contributions are twofold: First, we introduce a reverse-expansion-forward-inference strategy that facilitates the generation of interleaved image-text chains of thought for process-level supervision, which in turn leads to the construction of the **SIF-50K** dataset. Besides, we propose **GRPO-SIF**, a reinforced training paradigm that integrates depth-informed visual grounding into a unified reasoning pipeline, teaching the model to dynamically correct and focus on prompt-relevant regions. Extensive experiments demonstrate that *SIFThinker* outperforms state-of-the-art methods in spatial understanding and fine-grained visual perception, while maintaining strong general capabilities, highlighting the effectiveness of our method. Code: <https://github.com/zhangquanchen/SIFThinker>.

Introduction

Visual understanding is a fundamental task in computer vision, enabling machines to perceive, interpret, and interact with their surroundings (Wolfe and Horowitz 2017; Guo et al. 2016; Palmeri and Gauthier 2004). Traditional methods typically process the entire image in a uniform manner (Chen et al. 2024b, 2025b; Jiao et al. 2025; Shao et al. 2024a; Zhang et al. 2024), without considering the dynamic attention shifts and the underlying spatial awareness. However, an RGB image is inherently the 2D projection of 3D world, and human perception is dynamic attention shifts rooted in 3D awareness. For example, when prompted to identify the color of shirt worn by the person behind the tree, humans do not perceive the scene in a single step. They first

locate a coarse region of interest within their field of view. Then, they progressively focus on the tree while considering its 3D spatial relationship to the surroundings in mind. Finally, they correct their attention to the area behind the tree to determine the color of the shirt worn by the person.

The above observations indeed reveal two critical points in designing a human-like visual understanding framework – 1) **Dynamic visual perception**, which enables attention correction and facilitates focusing on prompt-relevant regions throughout the reasoning process; and 2) **3D spatial awareness**, which grounds visual perception within a spatial context. Moreover, *these two points can be naturally integrated into a unified framework*.

For the former, dynamic visual perception was initially pursued through reasoning frameworks. Early efforts, such as V* (Wu and Xie 2024), VisCoT (Shao et al. 2024b), and VisRL (Chen, Luo, and Li 2025), incorporated visual inputs into the reasoning paradigm in a stepwise manner: first predicting bounding boxes, then performing further inference based on the cropped image. This kind of fragmented method often severs the continuity of the reasoning chain, leading to weaker interpretability and incoherent anchoring of visual regions. More recent think-with-images methods, such as Cogcom (Qi et al. 2024) and ChatGPT-o3 (OpenAI 2025), utilize specialized-model-based or tool-based adaptive zooming to simulate dynamic attention. However, these methods are not intrinsic and heavily rely on external capabilities. In contrast, *SIFThinker intrinsically supports coherent image-text interleaved reasoning by simulating human-like visual attention correction and focusing*.

For the latter, the limitation primarily arises from the insufficient modeling of spatial information in MLLMs, i.e., most of them are pre-trained on RGB images paired with textual data without explicit spatial cues. Humans, on the other hand, are often capable of inferring 3D relationships from a single 2D image, enabling a deeper understanding of visual scenes. Prior works such as SpatialBot (Cai et al. 2024) and SSR (Liu et al. 2025b) attempt to equip models with 3D perception via data-driven or tool-based approaches. However, In real-world interactive scenarios, attention is seldom global. In contrast, *we typically perceive the spatial information (e.g., depth) of the prompt-relevant regions rather than the entire image*.

Moreover, previous works often fail to *integrate fine-*

*The work was conducted during the internship of Zhangquan Chen at ByteDance.

†Corresponding authors: ruqihuang@sz.tsinghua.edu.cn, yangyangkang@bytedance.com

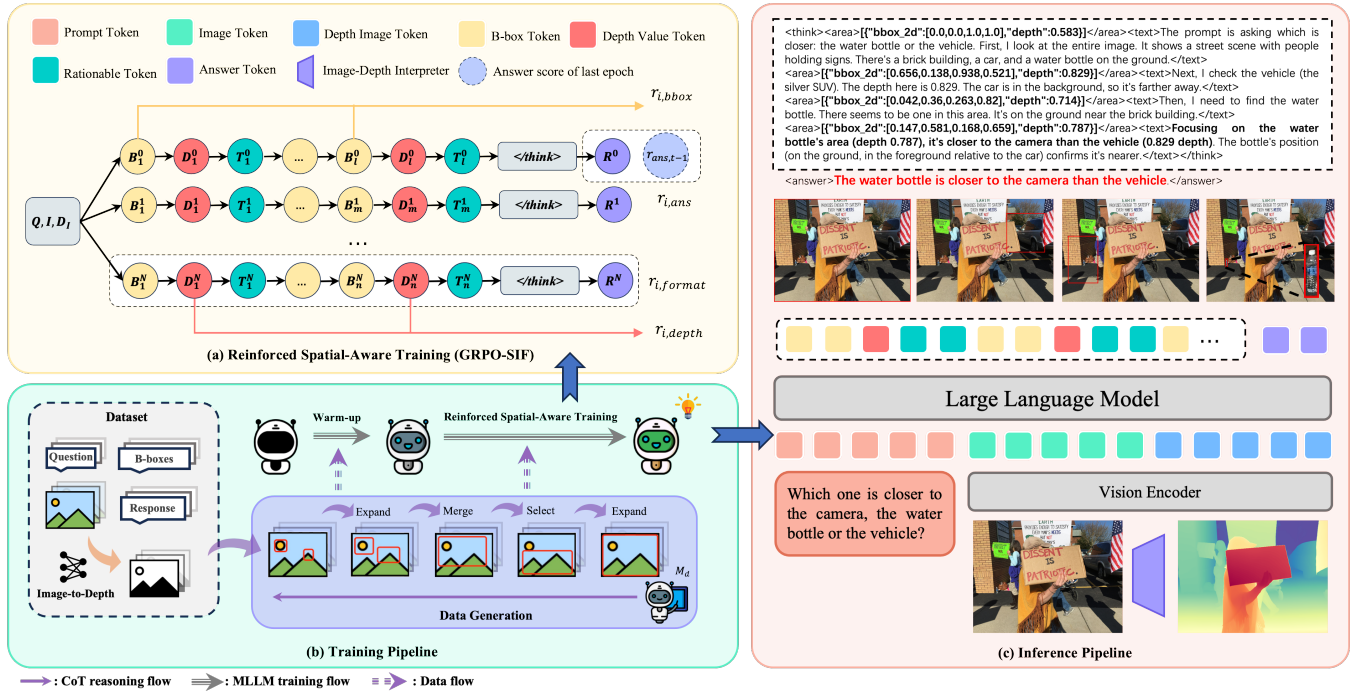


Figure 1: The schematic illustration of *SIFThinker*. (a) We propose a spatially-aware image focus paradigm, in which four novel reward functions are introduced under the RL framework to guide the optimization process. (b) The training pipeline of *SIFThinker* is illustrated, which builds upon our proposed data generation pipeline. It begins with a warm-up stage, followed by GRPO-SIF as described in (a). (c) illustrates the inference pipeline of our method given a question-image input.

grained visual perception with spatial awareness, and typically separate visual grounding from answer generation (e.g., VLM-R1 (Shen et al. 2025)). In contrast, we argue that 3D perception serves as a fundamental basis for deeper visual understanding. Besides, grounding-conditioned reasoning facilitates more accurate answer derivation, while result-level supervision can guide the correction of bounding boxes. Thus, there is a need for a spatially-aware, visually grounded reasoning process that offers a more coherent, unified, and effective framework for visual understanding.

To this end, we propose an adaptive image focus mechanism with 3D awareness, enabling the model to selectively and dynamically perceive the focused region with depth throughout the reasoning process. That is, we *integrate visual perception and spatial awareness into a unified grounded reasoning pipeline*.

Our method consists of three components: data generation, warm-up, and reinforcement learning (RL). In the data generation stage, we propose a novel image-text interleaved chain-of-thought (CoT) generation scheme that simulates spatially-aware visual focus. The constructed data support the warm-up stage via supervised fine-tuning (SFT), guiding the model to adopt structured interleaved reasoning. In the reinforcement learning stage, we go beyond outcome-only rewards and integrate format, depth estimation, region grounding, and answer prediction for each rollout.

Our main contributions can be summarized as follows.

- We present *SIFThinker*, the first framework to incorporate an adaptive focus mechanism with 3D awareness, enabling spatially grounded visual reasoning.
- We introduce a novel reverse-expansion-forward-inference strategy for constructing image-text inter-

leaved CoTs, and release the **SIF-50K** dataset for process-level supervision.

- We propose **GRPO-SIF**, which applies reinforcement learning for spatially-aware image focus training: 1) for visual grounding, we propose *HIOU*, a hierarchical design that better accommodates multiple objects, along with an effective reward formulation for bounding box correction; 2) for spatial awareness, we embed depth estimation into the model’s autoregressive structure; 3) we further design a progressive reward to encourage performance improvement across training epochs.
- Extensive experiments demonstrate that *SIFThinker* outperforms prior state-of-the-art methods in both fine-grained visual perception and spatial intelligence, while maintaining stable general capabilities—highlighting the robustness and broad applicability of our method.

Related Work

Visual Chain-of-Thought Reasoning

Recent studies have shown that step-by-step reasoning through in-context learning can significantly enhance the performance of large language models (LLMs). Accordingly, several approaches have emerged that aim to strengthen the visual reasoning capabilities of multi-modal large language models by introducing chain-of-thought strategies. These approaches can be categorized into three types: (T1) Pure-Text-Thought Methods: (Chen et al. 2025a; Thawakar et al. 2025; Ji et al. 2024; Hu et al. 2024; Shen et al. 2025; Bai et al. 2025b) elicit purely textual CoT reasoning within MLLMs for visual reasoning tasks inspired by (Guo et al. 2025b). They employ reinforcement learning

to guide the generation process towards final answers without explicitly incorporating intermediate visual signals. (T2) Intermediate-Thought Methods: (Liu et al. 2025a; Shao et al. 2024b; Chen, Luo, and Li 2025; Wang et al. 2024) first generate fine-grained visual cues (e.g, bounding boxes, spatial coordinates, or segmentation masks), CoT reasoning is then conducted based on these fine-grained visual cues. (T3) Multi-Modal-Thought Methods: Some recent methods aim to integrate visual-textual reasoning more tightly into the model’s thought process. Proprietary systems such as ChatGPT-o3 (OpenAI 2025) demonstrate the ability to “think-with-images” by dynamically invoking external image tools. Similarly, (Li et al. 2025) enables visual thinking by generating visual traces of reasoning. (Su et al. 2025; Wu et al. 2025; Zheng et al. 2025) optimize tool-usage ability via reinforcement learning. Moreover, (Zhang et al. 2025) iteratively crops the image based on generated bounding boxes to extract new visual cues for reasoning. (Fan et al. 2025) takes a more direct approach by generating reasoning chains that interleave natural language and explicit bounding boxes.

However, existing methods still exhibit several limitations: (T1) they rely heavily on textual reasoning, neglecting the dynamic visual attention shifts during the reasoning process; (T2) they produce less interpretable and often incoherent reasoning chains; and (T3) Some depend on external tools, specialized detection models or unstable image generation, while others overlook intermediate visual signals, relying solely on outcome-based supervision. Therefore, there is a need for an adaptive and coherent intrinsic method that enables visual-grounded reasoning—allowing MLLMs not only think “about” images, but also *dynamically focus, and correct their visual attention across image regions in a human-like manner*.

Spatial Intelligence

Existing MLLMs (Wu et al. 2024; Driess et al. 2023; Li et al. 2023b; Chen et al. 2022) are primarily trained on RGB images paired with textual data, which inherently lacks 3D spatial information. As a result, they demonstrate limited performance on tasks requiring spatial reasoning. To address this limitation, recent efforts such as SpatialRGPT (Cheng et al. 2024) and SpatialVLM (Chen et al. 2024a) have enhanced the spatial reasoning capabilities of MLLMs by constructing specialized spatially-oriented question-answering datasets and fine-tuning models accordingly. To further emphasize integrated reasoning capabilities, SSR (Liu et al. 2025b) incorporates depth images as additional inputs, while SpatialBot (Cai et al. 2024) leverages depth estimation tools to acquire spatial priors in key perceptual regions. However, these spatial perception approaches focus solely on reasoning, without achieving a deep integration with visual grounding—*two processes that are fundamentally interdependent in human visual perception*.

Methodology

As shown in Fig. 1, *SIFThinker* incorporates depth-enhanced focused regions of the image into the thinking process, enabling spatially grounded visual focus. *SIFThinker*

can iteratively analyze and refine the regions of interest, ultimately delivering a more accurate final response. In the following sections, we provide a detailed description of the data generation pipeline, the spatially-aware image focus training paradigm, and the **GRPO-SIF**.

Data Generation

To simulate the way humans observe spatial scenes, we model a focus mechanism that incorporates depth for data generation. That is, we construct **SIF-50K**, a dataset consisting of two parts: (1) a tailored fine-grained reasoning subset derived from spatial scenes in Flickr30k (Plummer et al. 2015), Visual7W (Zhu et al. 2016), GQA (Hudson and Manning 2019), Open Images (Kuznetsova et al. 2020), VSR (Liu, Emerson, and Collier 2023), and Birds-200-2021 (Wah et al. 2011), based on VisCoT (Shao et al. 2024b); and (2) a multi-instances subset resampled from Tal-lyQA (Acharya, Kafle, and Kanan 2019). All source datasets include ground-truth bounding boxes (b-boxes) annotations.

As illustrated in Alg. 1, given each question-image-bboxes-answer pairs (Q, I, B_{gt}, R) , we apply a reverse expansion procedure, followed by forward reasoning over the expanded regions based on DepthAnythingV2 (Yang et al. 2024) and Doubao-1.5-vision-pro (Guo et al. 2025a). This process yields the final SIF-50K dataset, denoted as $\mathcal{P} = \{(Q, I, D_I, B_{gt}, R, R_{cot})\}$.

Algorithm 1: Reverse Expansion for CoT Completion

Input: One sample from the source dataset including question Q , image I , normalized b-boxes B_{gt} , and response R .
Doubao-1.5-vision-pro model \mathcal{M}_d . DepthAnythingV2 model \mathcal{M}_{DA} .

Output: Completed reasoning chain R_{cot} .

```

1  $B_0 \leftarrow B_{gt}; \mathcal{B} \leftarrow \{B_0\}; ET \leftarrow False; K = 5; \mathcal{T} = 0.2$ 
  // Iteratively expand and merge b-boxes
2 for  $t \leftarrow 1$  to  $K$  do
3    $S \leftarrow K - t + 1; B_t \leftarrow \emptyset$ 
4   foreach  $b\text{-box } b = (x_1, y_1, x_2, y_2) \in B_{t-1}$  do
5      $\delta x_1 \leftarrow \frac{x_1}{S}, \delta x_2 \leftarrow \frac{1-x_2}{S}, \delta y_1 \leftarrow \frac{y_1}{S}, \delta y_2 \leftarrow \frac{1-y_2}{S}$ 
6      $b' \leftarrow (x_1 - \delta x_1, y_1 - \delta y_1, x_2 + \delta x_2, y_2 + \delta y_2)$ 
7      $B_t \leftarrow B_t \cup \{b'\}$ 
8   for each pair  $(b_i, b_j) \in B_t$  where  $IOU(b_i, b_j) > 0$  do
9      $b_{merged} \leftarrow$ 
       $(\min_{k \in \{i,j\}} x_1^k, \min_{k \in \{i,j\}} y_1^k, \max_{k \in \{i,j\}} x_2^k, \max_{k \in \{i,j\}} y_2^k)$ 
10     $B_t \leftarrow (B_t \setminus \{b_i, b_j\}) \cup \{b_{merged}\}$ 
11   $\mathcal{B} \leftarrow \mathcal{B} \cup \{B_t\}$ 
  // Early terminate
12  if  $|\mathcal{B}| = 1$  and not  $ET$  then
13     $K \leftarrow t + 2, ET \leftarrow True$ 
14  for  $i \leftarrow 1$  to random choice from  $\{0, 1, 2\}$  do
  //  $\mathcal{U}_I(\mathcal{B})$ : A set of b-boxes outside  $\mathcal{B}$ ;  $\mathcal{R}_{\mathcal{T}}(\cdot)$ :
  // Random selection with an area difference
  // no more than  $\mathcal{T}$ 
15     $B_{K+i} = \mathcal{R}_{\mathcal{T}}(\mathcal{U}_I(\bigcup_{j=K}^{K+i-1} B_j)); \mathcal{B} \leftarrow \mathcal{B} \cup \{B_{K+i}\}$ 
  // Reverse b-boxes set to generate CoT
16   $\mathcal{B}_{rev} \leftarrow \text{reverse}(\mathcal{B}); I_{seq} \leftarrow \text{DrawBBBoxes}(I, \mathcal{B}_{rev})$ 
17   $D_I \leftarrow \mathcal{M}_{DA}(I); R_{cot} \leftarrow \mathcal{M}_d(Q, R, D_I, (I_{seq}, \mathcal{B}_{rev}))$ 
18 return  $R_{cot}$ 

```

Spatially-aware image focus training paradigm

Method overview. We propose a two-stage pipeline to incorporate spatially-aware grounded reasoning. The first stage is a warm-start supervised fine-tuning phase, which biases the model to generate structured reasoning chains with explicitly focused regions, resulting in \mathcal{M}_{SFT} . This is followed by a reinforcement learning phase that further refines and optimizes these grounded behaviors, yielding the final model \mathcal{M}_{RL} . For SFT, we utilize the full set from SIF-50K to get $\mathcal{P}_{SFT} = (Q, I, D_I, R_{cot})$. For RL (detailed in the following section), to promote progressive learning with minimal supervision, we sample 200 instances from SIF-50K to form a smaller set $\mathcal{P}_{RL} = (Q, I, D_I, B_{gt}, R)$.

Reinforcement Learning with GRPO-SIF

RL Formulation. Built upon the Group-Relative Policy Optimisation (GRPO) (Shao et al. 2024c), the model \mathcal{M}_{SFT} is framed as a policy π_θ that generates an output sequence conditioned on the input (Q, I, D_I) . During training, for each question-image-depthimage pair (Q, I, D_I) , GRPO-SIF sample a set of N candidate completions $\{o_1, \dots, o_N\}$ from the current policy $\pi_{\theta_{old}}$, and then updates the current policy π_θ by maximizing the following objective:

$$\mathcal{J}(\theta) = \frac{1}{N} \sum_{i=1}^N \frac{1}{|o_i|} \sum_{t=1}^{|o_i|} \left\{ \min \left[\text{clip}(r_{i,t}, 1 - \epsilon, 1 + \epsilon) \hat{A}_{i,t}, r_{i,t} \hat{A}_{i,t} \right] - \beta \mathbb{D}_{KL}[\pi_\theta \parallel \pi_{ref}] \right\},$$

where $r_{i,t} = \frac{\pi_\theta(o_{i,t}|q, o_{i,<t})}{\pi_{\theta_{old}}(o_{i,t}|q, o_{i,<t})}$ denotes the ratio between the new and old policies at step t , ϵ and β are hyperparameters. $\mathbb{D}_{KL}[\pi_\theta \parallel \pi_{ref}]$ estimate the KL divergence with the unbiased estimator (Schulman 2020) between current policy model and the reference model. For each completion o_i , a task-specific reward $r_{i,t} = R(Q, I, D_I, B_{gt}, R, o_i)$ is computed based on a combination of reward components (detailed below) at step t . These rewards are then used to compute a group-normalized advantage:

$$\hat{A}_{i,t} = \frac{r_{i,t} - \text{mean}\{r_{1,t}, \dots, r_{N,t}\}}{\text{std}\{r_{1,t}, \dots, r_{N,t}\} + \delta}. \quad (1)$$

δ is a small constant (e.g., 10^{-8}) added for numerical stability. The task reward $r_{i,t}$ is a composite signal comprising four components: a spatially-aware grounded reasoning-format reward (r_{format}), a progressive-answer-accuracy reward ($r_{\text{ans},t}$), a correction-enhanced-grounding reward (r_{bbox}), and depth-consistency reward (r_{depth}). These components are designed to jointly encourage spatially-aware grounded reasoning, thus attaching the precise answer.

Hierarchical Intersection over Union ($HIoU$). To comprehensively reward the grounding quality between predicted b-boxes $B_p = \{b_1^p, b_2^p, \dots, b_n^p\}$ and ground-truth b-boxes $B_{gt} = \{b_1^{gt}, b_2^{gt}, \dots, b_m^{gt}\}$, we propose the Hierarchical IoU ($HIoU$) as shown in Fig. 2. This design mitigates reward hacking issues such as inflated AP reward scores by

incorporating both global and instance-level complementary components. (1) We first compute the global IoU ($GIoU$), which quantifies the overall spatial consistency between the predicted b-boxes and ground-truth b-boxes as a whole:

$$GIoU = \frac{\left| \bigcup_{b_i^p \in B_p} b_i^p \cap \bigcup_{b_j^{gt} \in B_{gt}} b_j^{gt} \right|}{\left| \bigcup_{b_i^p \in B_p} b_i^p \cup \bigcup_{b_j^{gt} \in B_{gt}} b_j^{gt} \right|}. \quad (2)$$

(2) Next, we compute a pairwise IoU via one-to-one bipartite matching between predicted b-boxes and ground-truth b-boxes using the Kuhn-Munkres algorithm (Kuhn 1955). Let $\mathcal{M}' \subseteq B_p \times B_{gt}$ denote the optimal matching set that maximizes the total IoU:

$$\mathcal{M} = \arg \max_{\mathcal{M}' \subseteq B_p \times B_{gt}} \sum_{(i,j) \in \mathcal{M}'} \text{IoU}(b_i^p, b_j^{gt}), \quad (3)$$

s.t. \mathcal{M}' is one-to-one.

The pairwise IoU ($PIoU$) score is then computed as the average over the matched pairs:

$$PIoU = \frac{1}{|\mathcal{M}|} \sum_{(i,j) \in \mathcal{M}} \frac{|b_i^p \cap b_j^{gt}|}{|b_i^p \cup b_j^{gt}|}. \quad (4)$$

The final $HIoU$ is computed as the average of the global and pairwise IoU accuracy.

$$HIoU = \frac{GIoU + PIoU}{2}. \quad (5)$$

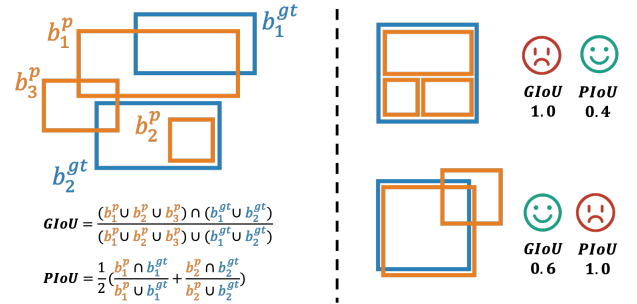


Figure 2: Visualization of our proposed $HIoU$ (left). The performance of $GIoU$ and $PIoU$ are illustrated respectively (right), highlighting the robustness against reward hacking.

Reasoning-format reward (r_{format}). This reward encourages the model to generate reasoning outputs structured with the designated special token, specifically adhering to the format: `<think><area>...</area><text>...</text></think><answer>...</answer>`. The `<area>...</area>` must contain a JSON-formatted representation of bounding boxes with depth, while `<text>...</text>` provides an explanation grounded in the specified spatial region. A reward of 1.0 is assigned to responses that strictly comply with this format.

Progressive-answer-accuracy reward ($r_{\text{ans},t}$). This reward integrates both the correctness of the final answer and the progression of answer quality over time, yielding a more robust signal than purely rule-based evaluations. Specifically, we leverage an external Vision-Language

Model (*Doubao-1.5-vision-pro*) as the judge to assess response quality. The reward is defined as:

$$r_{\text{ans},t} = s_t + (s_t - \text{mean}\{s_{1,t-1}, \dots, s_{N,t-1}\}) \quad (6)$$

where s_t denotes the continuous score assigned by the Doubao judge at step t , based on the question, the predicted answer, and the ground-truth answer. The term $(s_t - \text{mean}\{s_{1,t-1}, \dots, s_{N,t-1}\})$ captures the improvement between consecutive steps, thereby encouraging progressive refinement of the model’s responses. The evaluation prompt used by the judge is provided in the Supp. Mat..

Correction-enhanced grounding reward (r_{bbox}). Given the structured nature of our output format, we can explicitly extract the sequence of bounding boxes generated during the reasoning process, thereby enabling fine-grained tracking of the step-by-step grounding. Let B_{ini} denote the first bounding boxes in the reasoning trajectory that does not cover the entire image (i.e., $[0, 0, 1, 1]$), and let B_{end} denote the final bounding boxes in the sequence. To assess the accuracy of the grounding results, we compute two intermediate metrics: (1) the $HIoU$ between the final box B_{end} and the ground-truth box B_{gt} , denoted as $s_{\text{end}} = HIoU(B_{\text{end}}, B_{\text{gt}})$; and (2) the $HIoU$ between the initial box B_{ini} and B_{gt} , denoted as $s_{\text{init}} = HIoU(B_{\text{ini}}, B_{\text{gt}})$. The overall grounding reward consists of two components: the final grounding accuracy s_{end} and a correction-aware improvement term, defined as the relative gain $s_{\text{end}} - s_{\text{init}}$:

$$r_{\text{bbox}} = s_{\text{end}} + (s_{\text{end}} - s_{\text{init}}). \quad (7)$$

Depth-consistency reward (r_{depth}). A spatially-aware model is expected to accurately capture the depth value associated with each specified region. However, the presence of hallucinations may cause the autoregressively generated next-token to become inconsistent with the actual input depth image, resulting in spatial confusion. To address this, we perform step-wise verification on the depth tokens generated during the reasoning process. Specifically, for each b-boxes-depth pair (B_i, d_i) , we extract the corresponding ground-truth depth d_i^{gt} from the depth map D_I based on B_i , and require the absolute error to be less than the threshold $\mathcal{T} = 0.1$. A reward is assigned only when all depth values throughout the reasoning trajectory meet this consistency criterion.

$$r_{\text{depth}} = \mathbb{I}\left(\forall i : \frac{|d_i - d_i^{\text{gt}}|}{d_i^{\text{gt}}} \leq \mathcal{T}\right), \quad (8)$$

where $\mathbb{I}(\cdot)$ is the indicator function.

Experiments

We evaluate *SIFThinker* with several state-of-the-art (SOTA) methods on an array of different categories as follows. More details about datasets and the evaluation metric are listed in Supp. Mat..

Spatial Intelligence

We evaluate our method against several SOTA methods on a range of spatial understanding benchmarks. Benefiting from

| Model | SpatialBench | | | | SAT-Static | CV-Bench |
|-----------------------|--------------|-------------|-------------|-------------|-------------|-------------|
| | Pos. | Ext. | Cnt. | Size | | |
| o3-2025-04-16 | 79.4 | 95.0 | 89.9 | 35.0 | 67.4 | — |
| LLaVA-1.5-7B | 44.1 | 45.0 | 82.8 | 30.0 | 49.8 | 51.7 |
| LLaVA-NeXT-7B | 47.1 | 75.0 | 84.0 | 20.0 | 54.1 | 62.7 |
| SpatialBot-3B | 50.0 | 80.0 | 86.7 | 25.0 | 61.5 | 65.1 |
| Emu3-8B | 47.1 | 20.0 | 10.0 | 25.0 | — | — |
| Bunny-8B | 50.0 | 75.0 | 90.4 | 25.0 | 60.8 | 61.0 |
| SpatialBot-8B | 53.0 | 75.0 | 90.4 | 20.0 | — | — |
| <i>SIFThinker</i> -8B | 61.8 | 80.0 | 92.2 | 23.3 | 67.9 | 65.6 |
| Qwen2.5-VL-7B | 61.8 | 80.0 | 87.1 | 30.0 | 65.5 | 73.0 |
| SSR-7B | 64.7 | 85.0 | 90.2 | 28.3 | — | 73.3 |
| <i>SIFThinker</i> -7B | 73.5 | 95.0 | 94.7 | 35.0 | 72.8 | 75.9 |

Table 1: **Spatial perception evaluation** on SpatialBench (Position, Existence, Counting, Size), SAT (Static), and CV-Bench. Bunny-LLaMA3-8B and Qwen2.5-VL-7B serve as base models in the 3-rd and 4-th groups, respectively. The **best** is highlighted.

our spatially-aware think-with-images training paradigm, our model demonstrates superior 3D understanding capabilities. As shown in Tab. 1, under the same base model, our method outperforms SpatialBot (Cai et al. 2024) by **7.82%** (64.3 vs. 59.6) and SSR (Liu et al. 2025b) by **11.17%** (74.5 vs. 67.1) on SpatialBench (Cai et al. 2024). Furthermore, we evaluate our method on larger-scale benchmarks, SAT (Static) (Ray et al. 2024) and CV-Bench (Tong et al. 2024), achieving gains of **11.15%** (72.8 vs. 65.5) and **3.97%** (75.9 vs. 73.0) over the Qwen2.5-VL-7B base model, respectively. Although both SpatialBot and SSR incorporate depth images to enhance spatial understanding, *we argue that depth perception and spatial grounding are inherently complementary*. By introducing reasoning over spatially grounded regions, our method achieves more significant improvements.

We further conducted a comparison with the representative SOTA closed-source model—ChatGPT-o3 (OpenAI 2025). On SpatialBench, *SIFThinker* achieves a comparable average score to o3 (74.6 vs. 74.8). Notably, on SAT-Static, our method even outperforms o3 by a significant margin of **8.01%** (72.8 vs. 67.4), demonstrating the superior capability of *SIFThinker* in spatial perception.

Visual Perception

In this section, we comprehensively evaluate the visual perception capabilities of the method in terms of visual understanding, grounding capability and self-correction ability.

Visual Understanding. We select scene-related (e.g. non-planar) subsets from the VisCoT as VisCoT_s, and choose the attribute and spatial subsets from V*Bench. As shown in Tab. 2, on VisCoT_s dataset, under the same base model – LLaVA-1.5-7B, *SIFThinker* outperforms VisCoT by **11.76%** (0.751 vs. 0.672). Taking Qwen2.5-VL-7B as the base model for training, we surpass VisRL by **8.89%** (0.760 vs. 0.698). V*Bench presents a more challenging evaluation of fine-grained perception on high-resolution images. Remarkably, our method outperforms the state-of-the-art method – SEAL by **5.75%** on the Attribute subset (0.791 vs. 0.748), and by **1.70%** on the Spatial subset (0.776 vs. 0.763). In contrast to VisCoT, VisRL and SEAL, *SIFThinker* does not rely on a staged crop-image process.

| Model | VisCoT _s | | | | | V*Bench | | |
|---|---------------------|--------------|--------------|--------------|--------------|--------------|--------------|--------------|
| | Flickr30k | GQA | Open images | VSR | CUB | Avg | Attribute | Spatial |
| o3-2025-04-16 (OpenAI 2025) | 0.828 | 0.706 | 0.515 | 0.826 | 0.933 | 0.762 | 0.739 | 0.803 |
| LLaVA-1.5-7B (Liu et al. 2023) | 0.581 | 0.534 | 0.412 | 0.572 | 0.530 | 0.526 | 0.435 | 0.566 |
| VisCoT-LLaVA-1.5-7B (Shao et al. 2024b) | 0.671 | 0.616 | 0.833 | 0.682 | 0.556 | 0.672 | 0.466 | 0.571 |
| <i>SIFThinker</i> -LLaVA-1.5-7B | 0.749 | 0.675 | 0.801 | 0.698 | 0.831 | 0.751 | 0.565 | 0.671 |
| Qwen2.5-VL-7B (Bai et al. 2025a) | 0.601 | 0.467 | 0.289 | 0.581 | 0.583 | 0.504 | 0.644 | 0.634 |
| VisRL-Qwen2.5-VL-7B# (Chen, Luo, and Li 2025) | 0.662 | 0.589 | 0.767 | 0.698 | 0.698 | 0.772 | 0.678 | 0.658 |
| SEAL-7B (V*) (Wu and Xie 2024) | 0.723 | 0.599 | 0.448 | 0.730 | 0.640 | 0.628 | 0.748 | 0.763 |
| <i>SIFThinker</i> -Qwen2.5-VL-7B | 0.755 | 0.664 | 0.773 | 0.734 | 0.872 | 0.760 | 0.791 | 0.776 |

Table 2: **Visual perception performance** on VisCoT_s and V*Bench. # indicates methods trained on the same **SIF-43k** dataset as ours. For the same base models, the **best** is highlighted.

| Model | RefCOCO | | | RefCOCO+ | | | RefCOCOg | | OVDEval |
|---|-------------|-------------|-------------|-------------|-------------|-------------|-------------|-------------|-------------|
| | val | test-A | test-B | val | test-A | test-B | val-u | test-u | |
| UNIEXT (Yan et al. 2023) | 92.6 | 94.3 | 91.5 | 85.2 | 89.6 | 79.8 | 88.7 | 89.4 | — |
| Grounding-DINO (Liu et al. 2024a) | 90.6 | 93.2 | 88.2 | 82.8 | 89.0 | 75.9 | 86.1 | 87.0 | 25.3 |
| VisCoT-LLaVA-1.5-7B (Shao et al. 2024b) | 91.8 | 94.3 | 87.5 | 87.5 | 92.1 | 81.2 | 88.4 | 88.3 | — |
| Qwen2.5-VL-3B (Bai et al. 2025a) | 89.1 | 91.7 | 84.0 | 82.4 | 88.0 | 74.1 | 85.2 | 85.7 | 25.5 |
| Qwen2.5-VL-7B (Bai et al. 2025a) | 90.0 | 92.5 | 85.4 | 84.2 | 89.1 | 76.9 | 87.2 | 87.2 | 29.1 |
| VLM-R1-Qwen2.5-VL-3B (Shen et al. 2025) | 91.2 | 92.9 | 87.3 | 84.8 | 88.1 | 76.8 | 87.8 | 87.9 | 31.0 |
| VLM-R1-Qwen2.5-VL-7B# (Shen et al. 2025) | 90.9 | 93.4 | 87.5 | 85.0 | 88.6 | 77.2 | 88.2 | 88.3 | 26.3 |
| VisRL-Qwen2.5-VL-7B# (Chen, Luo, and Li 2025) | 92.3 | 94.2 | 88.9 | 84.4 | 89.5 | 77.8 | 88.5 | 89.1 | 25.9 |
| <i>SIFThinker</i> -Qwen2.5-VL-7B | 93.8 | 95.1 | 90.4 | 86.0 | 90.7 | 80.5 | 90.4 | 90.6 | 37.8 |

Table 3: Performance (Top-1 Accuracy@0.5) on Referring Expression Comprehension tasks and performance (NMS-AP) on Open-Vocabulary Detection tasks. # indicates methods trained on the same **SIF-43k** dataset as ours. The **best** is highlighted.

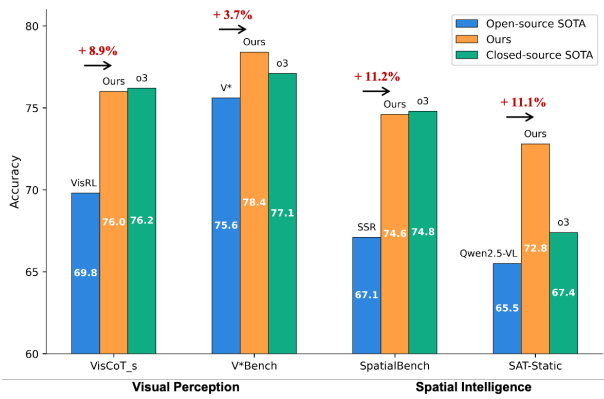


Figure 3: Comparison with other open-source SOTA methods (blue) under various benchmarks in terms of the same base model. Besides, we also include the performance of the proprietary SOTA model ChatGPT-o3-2025-04-16 (green).

ChatGPT-o3 leverages an external image magnification tool to explicitly capture fine-grained regions within the image. In contrast, *SIFThinker* adopts an intrinsic integration of visual information without any external tools. As shown in Tab. 2, a detailed comparison reveals that our method achieves comparable overall performance to o3 on the VisCoT_s benchmarks (0.760 vs. 0.762). Furthermore, on V*Bench-Attribute, our method surpasses o3 by a substantial margin of **7.04%** (0.791 vs. 0.739), highlighting the effectiveness in fine-grained visual reasoning. Instead, *SIFThinker* integrates visual perception directly into the thinking process with dynamically evolving bounding boxes to represent shifts in attention. This results in a more unified and intrinsically coherent reasoning approach. Furthermore, we explicitly incorporate 3D spatial information, which

brings additional benefits to scene-level grounding.

Grounding Capability. Since the accuracy of the final response is partly dependent on the correctness of the bounding boxes generated during the think process, we further evaluate the model’s grounding capability as shown in Tab. 3. Specifically, we select two structurally similar tasks—Referring Expression Comprehension (REC) and Open-Vocabulary Detection (OVD)—both of which require the model to generate bounding boxes conditioned on textual descriptions. *SIFThinker* outperforms all previous generalist models with comparable parameters, achieving an average improvement of **1% to 3%** over VisRL (93.08 vs. 91.78 on RefCOCO (Kazemzadeh et al. 2014), 85.76 vs. 83.90 on RefCOCO+ (Mao et al. 2016), 90.47 vs. 88.82 on RefCOCOg (Mao et al. 2016)). Moreover, in most of cases, *SIFThinker* even surpasses previous state-of-the-art specialist models (e.g. Grounding-DINO, UNINEXT). To further assess multi-object grounding performance of our method, we adopt OVDEval (Yao et al. 2023) with NMS-AP as the evaluation metric. Empowered by our proposed *HIOU*, *SIFThinker* exhibits promising robustness in multi-object scenarios, outperforming VisRL by **45.9%** (37.8 vs. 25.9).

Self-correction Ability. An effective image focus mechanism can simultaneously enable accurate attention correction. To this end, we also highlight the capability for bounding box correction shown in Fig. 4: given a starting focused area, *SIFThinker* is able to judge, search, and ultimately attend to the prompt-relevant area. Furthermore, we compare the visualized results of *SIFThinker* (red b-boxes) with VisRL (green b-boxes) and VLM-R1 (blue b-boxes) on the OVD task. *SIFThinker* successfully detects multiple relevant objects, while both VisRL and VLM-R1 yield only single-object predictions. This further highlights the multi-object

| Model | MME ^P | MME ^C | MMB ^T | MMB ^D | SEED-IVQA ^{v2} | POPE | |
|-------------------|------------------|------------------|------------------|------------------|-------------------------|-------------|-------------|
| LLaVA | 1511 | 282 | 66.5 | 62.1 | 65.8 | 79.1 | 85.9 |
| VisCoT | 1454 | 308 | 69.2 | 66.6 | 66.0 | 81.3 | 86.0 |
| <i>SIFThinker</i> | 1531 | 295 | 69.3 | 62.8 | 66.0 | 81.6 | 86.6 |
| Bunny | 1574 | 342 | 73.7 | 74.2 | 72.3 | 80.5 | 85.2 |
| SpatialBot | 1576 | 333 | 75.8 | 74.8 | 72.4 | 80.9 | 85.3 |
| <i>SIFThinker</i> | 1580 | 355 | 76.8 | 75.0 | 72.5 | 81.8 | 85.7 |
| Qwen2.5VL | 1670 | 623 | 80.3 | 81.5 | 77.0 | 83.3 | 85.9 |
| <i>SIFThinker</i> | 1702 | 650 | 83.4 | 82.4 | 77.2 | 84.5 | 86.9 |

Table 4: Results on general VLM Benchmarks. Methods are grouped by their underlying base model: LLaVA-1.5-7B (top), Bunny-Llama3-8B (middle), and Qwen2.5-VL-7B (bottom). For each group, the **best** is highlighted.



Figure 4: Visualization of the *SIFThinker*'s region correction and detection (multi-objects) capabilities.

friendliness of *SIFThinker*.

Overall, as shown in Fig. 3, at the 7B parameter scale, *SIFThinker* (orange) exhibits strong reasoning capabilities in both spatial understanding and visual perception, outperforming all open-source models (blue) and approaching the performance of the larger-scale ChatGPT-o3 (green). Notably, *SIFThinker* even surpasses ChatGPT-o3 on V*Bench and SAT-Static.

General VLM Benchmarks

As shown in Tab. 4, we report results on widely used general benchmarks, including MME (Fu et al. 2024) perception (MME^P), MME cognition (MME^C), MMBench (Liu et al. 2024b) test and dev sets (denoted as MMB^T and MMB^D), SEED-Bench (Li et al. 2023a) images (SEED-I), VQA^{v2} (Goyal et al. 2017) test-dev split, and POPE (Li et al. 2023c) (measured as the average F1 score over three categories on the COCO validation set). Across most of these benchmarks, *SIFThinker* not only avoids performance degradation but even achieves notable improvements, demonstrating the robustness of our method—particularly in scenarios that depth information can benefit. Under the same base models, *SIFThinker* consistently outperforms both VisCoT, which focuses on fine-grained visual perception, and SpatialBot, which emphasizes spatial reasoning. Remarkably, on MMB^T, *SIFThinker* achieves about 4% improvements across different base model settings (69.3 vs. 66.5 on LLaVA-1.5-7B, 76.8 vs. 73.7 on Bunny-Llama3-8B, 83.4 vs. 80.3 on Qwen2.5-VL-7B).

| Model | VisCoT-s | | | | | |
|------------------------|--------------|--------------|--------------|--------------|--------------|--------------|
| | Flickr30k | GQA | Open images | VSR | CUB | Avg |
| VQA-SFT | 0.542 | 0.508 | 0.390 | 0.597 | 0.642 | 0.536 |
| CoT-SFT | 0.517 | 0.468 | 0.556 | 0.588 | 0.780 | 0.582 |
| w/o r_{bbox} | 0.641 | 0.580 | 0.711 | 0.705 | 0.839 | 0.695 |
| w/o $r_{\text{ans},t}$ | 0.628 | 0.573 | 0.658 | 0.663 | 0.795 | 0.663 |
| w/o D_I | 0.571 | 0.595 | 0.589 | 0.651 | 0.870 | 0.655 |
| w/o r_{depth} | 0.748 | 0.666 | 0.762 | 0.718 | 0.872 | 0.753 |
| Full | 0.755 | 0.664 | 0.773 | 0.734 | 0.872 | 0.760 |

Table 5: Performance on different ablated settings in terms of Qwen2.5-VL-7B.

Ablation Study

In this section, we present a comprehensive ablation study in Tab. 5. VQA-SFT refers to directly applying SFT on the original question-answer pairs, which serve as the source data from where **SIF-50K** was constructed, whereas CoT-SFT leverages the Chain-of-Thought (CoT) construction strategy introduced in Alg. 1. This demonstrates that guiding the model to think with images yields a notable performance improvement of **8.58%** (0.582 vs. 0.536). However, SFT alone mainly helps the model learn output formatting, and in some cases (e.g., GQA), even leads to performance degradation. In contrast, incorporating RL yields consistent and substantial improvements, achieving an additional **30.58%** gain over SFT alone (0.760 vs. 0.582). We further perform ablations on various RL rewards (w/o $r_{\text{ans},t}$, r_{bbox} , r_{depth}) and evaluate the impact of depth information (w/o D_I). The results suggest that the observed performance gains are primarily attributed to three key factors: 1) the think-with-images reasoning paradigm, which promotes spatially grounded cognition; 2) the carefully designed reward functions for both bounding box prediction and response generation, which work synergistically to encourage iterative correction and refinement; 3) the inclusion of depth inputs, which enhance the model's spatial intelligence during grounding. Together, these designs form a unified and robust framework for spatially-aware visual grounding, endowing the model with a general-purpose reasoning capability that improves performance across diverse benchmarks.

Conclusion and Limitation

In this paper, we propose *SIFThinker*, a spatially-aware image-text interleaved reasoning framework. Inspired by human-like prompt-driven search in 3D environments, *SIFThinker* performs spatially-aware grounding before delivering the final response. Specifically, we introduce a novel pipeline for generating CoT datasets tailored for think-with-images reasoning, enabling process-level supervision. Building on this dataset, we propose GRPO-SIF by incorporating not only region-level corrective signals, but also proposing progress learning and depth consistency rewards. Extensive experiments across diverse benchmarks demonstrate the effectiveness of *SIFThinker*.

Limitation & Future Work. Since *SIFThinker* is trained on single-image, it may face challenges in generalizing to dynamic spatial scenarios that require reasoning across multiple images. We believe extending it to such settings would be interesting for higher practical impact.

References

- Acharya, M.; Kafle, K.; and Kanan, C. 2019. Tallyqa: Answering complex counting questions. In *Proceedings of the AAAI conference on artificial intelligence*, volume 33, 8076–8084.
- Bai, S.; Chen, K.; Liu, X.; Wang, J.; Ge, W.; Song, S.; Dang, K.; Wang, P.; Wang, S.; Tang, J.; et al. 2025a. Qwen2. 5-VL Technical Report. *arXiv preprint arXiv:2502.13923*.
- Bai, S.; Li, M.; Liu, Y.; Tang, J.; Zhang, H.; Sun, L.; Chu, X.; and Tang, Y. 2025b. Univg-r1: Reasoning guided universal visual grounding with reinforcement learning. *arXiv preprint arXiv:2505.14231*.
- Cai, W.; Ponomarenko, I.; Yuan, J.; Li, X.; Yang, W.; Dong, H.; and Zhao, B. 2024. Spatialbot: Precise spatial understanding with vision language models. *arXiv preprint arXiv:2406.13642*.
- Chen, B.; Xu, Z.; Kirmani, S.; Ichter, B.; Sadigh, D.; Guibas, L.; and Xia, F. 2024a. Spatialvlm: Endowing vision-language models with spatial reasoning capabilities. In *Proceedings of the IEEE/CVF Conference on Computer Vision and Pattern Recognition*, 14455–14465.
- Chen, L.; Li, J.; Dong, X.; Zhang, P.; He, C.; Wang, J.; Zhao, F.; and Lin, D. 2024b. Sharegpt4v: Improving large multi-modal models with better captions. In *European Conference on Computer Vision*, 370–387. Springer.
- Chen, L.; Li, L.; Zhao, H.; Song, Y.; and Vinci. 2025a. R1-V: Reinforcing Super Generalization Ability in Vision-Language Models with Less Than \$3. <https://github.com/Deep-Agent/R1-V>. Accessed: 2025-02-02.
- Chen, L.; Wei, X.; Li, J.; Dong, X.; Zhang, P.; Zang, Y.; Chen, Z.; Duan, H.; Tang, Z.; Yuan, L.; et al. 2025b. Sharegpt4video: Improving video understanding and generation with better captions. *Advances in Neural Information Processing Systems*, 37: 19472–19495.
- Chen, X.; Wang, X.; Changpinyo, S.; Piergiovanni, A. J.; Padlewski, P.; Salz, D.; Goodman, S.; Grycner, A.; Mustafa, B.; Beyer, L.; et al. 2022. Pali: A jointly-scaled multilingual language-image model. *arXiv preprint arXiv:2209.06794*.
- Chen, Z.; Luo, X.; and Li, D. 2025. Visrl: Intention-driven visual perception via reinforced reasoning. *arXiv preprint arXiv:2503.07523*.
- Cheng, A.-C.; Yin, H.; Fu, Y.; Guo, Q.; Yang, R.; Kautz, J.; Wang, X.; and Liu, S. 2024. Spatialrgpt: Grounded spatial reasoning in vision-language models. *Advances in Neural Information Processing Systems*, 37: 135062–135093.
- Driess, D.; Xia, F.; Sajjadi, M. S.; Lynch, C.; Chowdhery, A.; Wahid, A.; Tompson, J.; Vuong, Q.; Yu, T.; Huang, W.; et al. 2023. Palm-e: An embodied multimodal language model.
- Fan, Y.; He, X.; Yang, D.; Zheng, K.; Kuo, C.-C.; Zheng, Y.; Narayanaraju, S. J.; Guan, X.; and Wang, X. E. 2025. GRIT: Teaching MLLMs to Think with Images. *arXiv preprint arXiv:2505.15879*.
- Fu, C.; Chen, P.; Shen, Y.; Qin, Y.; Zhang, M.; Lin, X.; Yang, J.; Zheng, X.; Li, K.; Sun, X.; Wu, Y.; and Ji, R. 2024. MME: A Comprehensive Evaluation Benchmark for Multimodal Large Language Models. *arXiv:2306.13394*.
- Goyal, Y.; Khot, T.; Summers-Stay, D.; Batra, D.; and Parikh, D. 2017. Making the v in vqa matter: Elevating the role of image understanding in visual question answering. In *Proceedings of the IEEE conference on computer vision and pattern recognition*, 6904–6913.
- Guo, D.; Wu, F.; Zhu, F.; Leng, F.; Shi, G.; Chen, H.; Fan, H.; Wang, J.; Jiang, J.; Wang, J.; et al. 2025a. Seed1. 5-vl technical report. *arXiv preprint arXiv:2505.07062*.
- Guo, D.; Yang, D.; Zhang, H.; Song, J.; Zhang, R.; Xu, R.; Zhu, Q.; Ma, S.; Wang, P.; Bi, X.; et al. 2025b. Deepseek-r1: Incentivizing reasoning capability in llms via reinforcement learning. *arXiv preprint arXiv:2501.12948*.
- Guo, Y.; Liu, Y.; Oerlemans, A.; Lao, S.; Wu, S.; and Lew, M. S. 2016. Deep learning for visual understanding: A review. *Neuro-computing*, 187: 27–48.
- Hu, J.; Wu, X.; Zhu, Z.; Xianyu; Wang, W.; Zhang, D.; and Cao, Y. 2024. OpenRLHF: An Easy-to-use, Scalable and High-performance RLHF Framework. *arXiv preprint arXiv:2405.11143*.
- Hudson, D. A.; and Manning, C. D. 2019. Gqa: A new dataset for real-world visual reasoning and compositional question answering. In *Proceedings of the IEEE/CVF conference on computer vision and pattern recognition*, 6700–6709.
- Ji, J.; Zhou, J.; Lou, H.; Chen, B.; Hong, D.; Wang, X.; Chen, W.; Wang, K.; Pan, R.; Li, J.; Wang, M.; Dai, J.; Qiu, T.; Xu, H.; Li, D.; Chen, W.; Song, J.; Zheng, B.; and Yang, Y. 2024. Align Anything: Training All-Modality Models to Follow Instructions with Language Feedback.
- Jiao, Y.; Chen, S.; Jie, Z.; Chen, J.; Ma, L.; and Jiang, Y.-G. 2025. Lumen: Unleashing versatile vision-centric capabilities of large multimodal models. *Advances in Neural Information Processing Systems*, 37: 81461–81488.
- Kazemzadeh, S.; Ordonez, V.; Matten, M.; and Berg, T. 2014. Referitgame: Referring to objects in photographs of natural scenes. In *Proceedings of the 2014 conference on empirical methods in natural language processing (EMNLP)*, 787–798.
- Kuhn, H. W. 1955. The Hungarian method for the assignment problem. *Naval research logistics quarterly*, 2(1-2): 83–97.
- Kuznetsova, A.; Rom, H.; Alldrin, N.; Uijlings, J.; Krasin, I.; Pont-Tuset, J.; Kamali, S.; Popov, S.; Mallocci, M.; Kolesnikov, A.; et al. 2020. The open images dataset v4: Unified image classification, object detection, and visual relationship detection at scale. *International journal of computer vision*, 128(7): 1956–1981.
- Li, B.; Wang, R.; Wang, G.; Ge, Y.; Ge, Y.; and Shan, Y. 2023a. Seed-bench: Benchmarking multimodal llms with generative comprehension. *arXiv preprint arXiv:2307.16125*.
- Li, C.; Wu, W.; Zhang, H.; Xia, Y.; Mao, S.; Dong, L.; Vulić, I.; and Wei, F. 2025. Imagine while Reasoning in Space: Multimodal Visualization-of-Thought. *arXiv preprint arXiv:2501.07542*.
- Li, J.; Li, D.; Savarese, S.; and Hoi, S. 2023b. Blip-2: Bootstrapping language-image pre-training with frozen image encoders and large language models. In *International conference on machine learning*, 19730–19742. PMLR.
- Li, Y.; Du, Y.; Zhou, K.; Wang, J.; Zhao, W. X.; and Wen, J.-R. 2023c. Evaluating object hallucination in large vision-language models. *arXiv preprint arXiv:2305.10355*.
- Liu, F.; Emerson, G.; and Collier, N. 2023. Visual spatial reasoning. *Transactions of the Association for Computational Linguistics*, 11: 635–651.
- Liu, H.; Li, C.; Li, Y.; and Lee, Y. J. 2023. Improved Baselines with Visual Instruction Tuning.
- Liu, S.; Zeng, Z.; Ren, T.; Li, F.; Zhang, H.; Yang, J.; Jiang, Q.; Li, C.; Yang, J.; Su, H.; et al. 2024a. Grounding dino: Marrying dino with grounded pre-training for open-set object detection. In *European Conference on Computer Vision*, 38–55. Springer.
- Liu, Y.; Chi, D.; Wu, S.; Zhang, Z.; Hu, Y.; Zhang, L.; Zhang, Y.; Wu, S.; Cao, T.; Huang, G.; et al. 2025a. SpatialCoT: Advancing Spatial Reasoning through Coordinate Alignment and Chain-of-Thought for Embodied Task Planning. *arXiv preprint arXiv:2501.10074*.

- Liu, Y.; Duan, H.; Zhang, Y.; Li, B.; Zhang, S.; Zhao, W.; Yuan, Y.; Wang, J.; He, C.; Liu, Z.; et al. 2024b. Mmbench: Is your multimodal model an all-around player? In *European conference on computer vision*, 216–233. Springer.
- Liu, Y.; Ma, M.; Yu, X.; Ding, P.; Zhao, H.; Sun, M.; Huang, S.; and Wang, D. 2025b. SSR: Enhancing Depth Perception in Vision-Language Models via Rationale-Guided Spatial Reasoning. *arXiv preprint arXiv:2505.12448*.
- Mao, J.; Huang, J.; Toshev, A.; Camburu, O.; Yuille, A. L.; and Murphy, K. 2016. Generation and comprehension of unambiguous object descriptions. In *Proceedings of the IEEE conference on computer vision and pattern recognition*, 11–20.
- OpenAI. 2025. Introducing OpenAI o3 and o4-mini. <https://openai.com/index/introducing-o3-and-o4-mini/>.
- Palmeri, T. J.; and Gauthier, I. 2004. Visual object understanding. *Nature Reviews Neuroscience*, 5(4): 291–303.
- Plummer, B. A.; Wang, L.; Cervantes, C. M.; Caicedo, J. C.; Hockenmaier, J.; and Lazebnik, S. 2015. Flickr30k entities: Collecting region-to-phrase correspondences for richer image-to-sentence models. In *Proceedings of the IEEE international conference on computer vision*, 2641–2649.
- Qi, J.; Ding, M.; Wang, W.; Bai, Y.; Lv, Q.; Hong, W.; Xu, B.; Hou, L.; Li, J.; Dong, Y.; et al. 2024. Cogcom: Train large vision-language models diving into details through chain of manipulations.
- Ray, A.; Duan, J.; Tan, R.; Bashkirova, D.; Hendrix, R.; Ehsani, K.; Kembhavi, A.; Plummer, B. A.; Krishna, R.; Zeng, K.-H.; et al. 2024. SAT: Spatial Aptitude Training for Multimodal Language Models. *arXiv preprint arXiv:2412.07755*.
- Schulman, J. 2020. Approximating kl divergence. *John Schulman's Homepage*.
- Shao, H.; Hu, Y.; Wang, L.; Song, G.; Waslander, S. L.; Liu, Y.; and Li, H. 2024a. Lmdrive: Closed-loop end-to-end driving with large language models. In *Proceedings of the IEEE/CVF Conference on Computer Vision and Pattern Recognition*, 15120–15130.
- Shao, H.; Qian, S.; Xiao, H.; Song, G.; Zong, Z.; Wang, L.; Liu, Y.; and Li, H. 2024b. Visual CoT: Unleashing Chain-of-Thought Reasoning in Multi-Modal Language Models. *arXiv:2403.16999*.
- Shao, Z.; Wang, P.; Zhu, Q.; Xu, R.; Song, J.; Bi, X.; Zhang, H.; Zhang, M.; Li, Y.; Wu, Y.; et al. 2024c. Deepseekmath: Pushing the limits of mathematical reasoning in open language models. *arXiv preprint arXiv:2402.03300*.
- Shen, H.; Zhang, Z.; Zhang, Q.; Xu, R.; and Zhao, T. 2025. VLM-R1: A stable and generalizable R1-style Large Vision-Language Model. <https://github.com/om-ai-lab/VLM-R1>. Accessed: 2025-02-15.
- Su, Z.; Li, L.; Song, M.; Hao, Y.; Yang, Z.; Zhang, J.; Chen, G.; Gu, J.; Li, J.; Qu, X.; et al. 2025. Openthinking: Learning to think with images via visual tool reinforcement learning. *arXiv preprint arXiv:2505.08617*.
- Thawakar, O.; Dissanayake, D.; More, K.; Thawkar, R.; Heakl, A.; Ahsan, N.; Li, Y.; Zumri, M.; Lahoud, J.; Anwer, R. M.; Cholakkal, H.; Laptev, I.; Shah, M.; Khan, F. S.; and Khan, S. 2025. LlamaV-o1: Rethinking Step-by-step Visual Reasoning in LLMs. *arXiv:2501.06186*.
- Tong, P.; Brown, E.; Wu, P.; Woo, S.; IYER, A. J. V.; Akula, S. C.; Yang, S.; Yang, J.; Middepogu, M.; Wang, Z.; et al. 2024. Cambrian-1: A fully open, vision-centric exploration of multimodal llms. *Advances in Neural Information Processing Systems*, 37: 87310–87356.
- Wah, C.; Branson, S.; Welinder, P.; Perona, P.; and Belongie, S. 2011. The caltech-ucsd birds-200-2011 dataset.
- Wang, X.; Zhang, S.; Li, S.; Kallidromitis, K.; Li, K.; Kato, Y.; Kozuka, K.; and Darrell, T. 2024. SegLLM: Multi-round Reasoning Segmentation. *arXiv preprint arXiv:2410.18923*.
- Wolfe, J. M.; and Horowitz, T. S. 2017. Five factors that guide attention in visual search. *Nature human behaviour*, 1(3): 0058.
- Wu, M.; Yang, J.; Jiang, J.; Li, M.; Yan, K.; Yu, H.; Zhang, M.; Zhai, C.; and Nahrstedt, K. 2025. VTool-R1: VLMs Learn to Think with Images via Reinforcement Learning on Multimodal Tool Use. *arXiv preprint arXiv:2505.19255*.
- Wu, P.; and Xie, S. 2024. V?: Guided visual search as a core mechanism in multimodal llms. In *Proceedings of the IEEE/CVF Conference on Computer Vision and Pattern Recognition*, 13084–13094.
- Wu, S.; Fei, H.; Qu, L.; Ji, W.; and Chua, T.-S. 2024. Next-gpt: Any-to-any multimodal llm. In *Forty-first International Conference on Machine Learning*.
- Yan, B.; Jiang, Y.; Wu, J.; Wang, D.; Luo, P.; Yuan, Z.; and Lu, H. 2023. Universal instance perception as object discovery and retrieval. In *Proceedings of the IEEE/CVF Conference on Computer Vision and Pattern Recognition*, 15325–15336.
- Yang, L.; Kang, B.; Huang, Z.; Zhao, Z.; Xu, X.; Feng, J.; and Zhao, H. 2024. Depth anything v2. *Advances in Neural Information Processing Systems*, 37: 21875–21911.
- Yao, Y.; Liu, P.; Zhao, T.; Zhang, Q.; Liao, J.; Fang, C.; Lee, K.; and Wang, Q. 2023. How to Evaluate the Generalization of Detection? A Benchmark for Comprehensive Open-Vocabulary Detection. *arXiv preprint arXiv:2308.13177*.
- Zhang, J.; Jiao, Y.; Chen, S.; Chen, J.; and Jiang, Y.-G. 2024. Eventhallusion: Diagnosing event hallucinations in video llms. *arXiv preprint arXiv:2409.16597*.
- Zhang, X.; Gao, Z.; Zhang, B.; Li, P.; Zhang, X.; Liu, Y.; Yuan, T.; Wu, Y.; Jia, Y.; Zhu, S.-C.; et al. 2025. Chain-of-Focus: Adaptive Visual Search and Zooming for Multimodal Reasoning via RL. *arXiv preprint arXiv:2505.15436*.
- Zheng, Z.; Yang, M.; Hong, J.; Zhao, C.; Xu, G.; Yang, L.; Shen, C.; and Yu, X. 2025. DeepEyes: Incentivizing “Thinking with Images” via Reinforcement Learning. *arXiv preprint arXiv:2505.14362*.
- Zhu, Y.; Groth, O.; Bernstein, M.; and Fei-Fei, L. 2016. Visual7w: Grounded question answering in images. In *Proceedings of the IEEE conference on computer vision and pattern recognition*, 4995–5004.

In this supplementary material, we provide more technical details and experimental results, including 1) the overview of our training dataset; 2) the benchmarks and evaluation metric used in this paper; 3) some implementation details in terms of experimental setup, hyper-parameters setup and prompt designs; and 4) more visualization of *SIFThinker*.

Training Dataset

We propose **SIF-50K** dataset for training based on our CoT data generation pipeline. The data are from VisCoT training set (Shao et al. 2024b) and TallyQA (Acharya, Kafle, and Kanan 2019), with each source sample containing a question, image, answer, and ground-truth bounding boxes. Dataset statistics are provided in Tab. 6.

Benchmarks

We conduct evaluations on a series of benchmarks, following the metric settings defined by each benchmark.

Spatial Intelligence

SpatialBench: We evaluate the spatial comprehension capabilities of MLLMs using SpatialBench (Cai et al. 2024), which contains manually annotated question-answer pairs focused on spatial understanding and reasoning. We use four categories: position (34 samples), existence (40 samples), counting (20 samples), and size (40 samples).

SAT (Static): The SAT (Ray et al. 2024) dataset includes both static and dynamic spatial reasoning tasks. We select the static evaluation subset (single-image), which contains 127405 samples.

CV-Bench: With 2,638 manually inspected samples, CV-Bench (Tong et al. 2024) includes four tasks: spatial relationship, object counting, depth order, and relative distance.

Visual Perception

VisCoT_s: VisCoT_s is the subset from VisCoT dataset (eval) (Shao et al. 2024b), comprising several scene-specific datasets (3D information may help), including Flickr30k (Plummer et al. 2015), VSR (Liu, Emerson, and Collier 2023), GQA (Hudson and Manning 2019), Open Images (Kuznetsova et al. 2020), and CUB (Wah et al. 2011). Specifically, Flickr30k (Plummer et al. 2015) dataset provides five human-written captions per image along with bounding box annotations for most referenced objects. Building upon this, (Shao et al. 2024b) further utilizes GPT-4 to generate questions that specifically target small objects. The Visual Spatial Reasoning (VSR) (Liu, Emerson, and Collier 2023), GQA (Hudson and Manning 2019), and Open Images (Kuznetsova et al. 2020) datasets are rich in spatial relational information between image entities. The Birds-200-2011 (CUB) (Wah et al. 2011) dataset is a widely adopted benchmark for fine-grained visual categorization, which contains high-resolution bird images along with detailed part annotations, attribute labels, and bounding boxes. To better exploit this dataset in the context of MLLMs, (Shao et al. 2024b) design probing questions that require the model to identify fine-grained bird characteristics, thereby assessing its capacity for detailed visual recognition.

V* Bench: To evaluate the performance of MLLMs in complex visual scenarios with dense, high-resolution imagery, we use V*Bench (Wu and Xie 2024), a benchmark of 191 images (avg. resolution: 2246×1582) comprising two tasks: attribute recognition (115 samples) and spatial relationship reasoning (76 samples). These tasks assess models’ fine-grained visual understanding.

Visual Grounding

RefCOCO/RefCOCO+/RefCOCOg: Referring Expression Comprehension (REC) can directly use the Intersection-over-Union (IoU) between the predicted and ground-truth bounding boxes as the explicit evaluation. Thus, We evaluate various methods on REC benchmarks, including RefCOCO (Kazemzadeh et al. 2014), RefCOCO+ (Mao et al. 2016), and RefCOCOg (Mao et al. 2016). RefCOCO and RefCOCO+ were collected via an interactive game and follow the standard val/testA/testB split, where testA focuses on people and testB on other objects. RefCOCO+ excludes absolute spatial terms from queries. RefCOCOg, collected non-interactively, features longer and more descriptive queries. We follow (Shao et al. 2024b) by setting the IoU threshold to 0.5 for accuracy evaluation, i.e., Top-1 Accuracy@0.5 as evaluation metric.

OVDEval: OVDEval (Yao et al. 2023) is a benchmark for the Open-Vocabulary Detection task, comprising 9 sub-tasks that evaluate commonsense reasoning, attribute and spatial understanding, object relations, etc.. Compared to RefCOCO/RefCOCO+/RefCOCOg, OVDEval supports multi-object grounding with multiple bounding box annotations. Additionally, we adopt the Non-Maximum Suppression Average Precision (NMS-AP) metric from OVDEval (Yao et al. 2023) for evaluation.

General VLM Benchmarks

We further evaluate the models on five general benchmarks, as summarized in Tab. 4 of the main text: MME(Fu et al. 2024), which assesses perception and cognition across 14 sub-tasks; MM-Bench(Liu et al. 2024b), a systematically designed benchmark covering 20 capability dimensions for robust, holistic evaluation; SEED-Bench (Li et al. 2023a), containing 19242 multiple-choice questions with high-quality human annotations—spanning 12 evaluation dimensions across image and video modalities; VQA (Goyal et al. 2017), a dataset of open-ended questions over 265016 images (from COCO and abstract scenes), requiring vision, language, and commonsense understanding; and POPE (Li et al. 2023c), which frames hallucination evaluation as binary object presence questions. More details about evaluation splits have been detailed in Sec. 4 of the main text.

Implementation details

Experimental Setup

We perform all the experiments on a machine with 8*NVIDIA H20 96GB and Intel(R) Xeon(R) Platinum 8457C with 180 cores.

Hyper-parameters setup

Taking Qwen2.5-VL-7B as an example, during the SFT stage, we utilized the full SIF-50k dataset, setting LORA rank (i.e., r) to 8, training for 3 epochs with a learning rate of $1e-4$. In the RL stage, we sampled only 200 samples from the SIF-50k dataset. We adopted the default GRPO hyperparameter settings, configuring N to 8, the KL divergence ratio (i.e., β) to 0.04, LORA rank (i.e., r) to 64, and trained for 20 epochs with a learning rate of $1e-5$. The maximum completion length was set to 2028 tokens for both the SFT and RL stages.

Prompt template

Here, we present the prompt designs employed in our method. Specifically, to enable *SIFThinker* to adopt a “think-with-images” generation paradigm, we employ the prompt shown in Fig. 5. During the final stage of the data generation pipeline, when a high-level model is used to complete the CoT reasoning, we apply the prompt

| Domain | Source Dataset | Size |
|----------------------------|--|--------------|
| Counting | Tallyqa (Acharya, Kafle, and Kanan 2019) | 370 |
| General VQA | Flickr30k (Plummer et al. 2015) | 9782 |
| | Visual7W (Zhu et al. 2016) | 8266 |
| Relation Reasoning | GQA (Hudson and Manning 2019) | 9481 |
| | Open images (Kuznetsova et al. 2020) | 8959 |
| | VSR (Liu, Emerson, and Collier 2023) | 3041 |
| Fine-Grained Understanding | Birds-200-2011 (Wah et al. 2011) | 9782 |
| Sum | | 49681 |

Table 6: The overview of the SIF-50K dataset. The dataset spans four distinct domains and includes various source datasets.

Thinking Prompt

Original image: <image>\nDepth image: <image>\n **{problem}**
Please first output the thinking process in <think> </think> tags, where bounding box with depth is enclosed in <area> </area> tags and text analysis is enclosed in <text> </text> tags, alternating between them to iteratively refine the focused area. Then output the final answer in <answer> </answer> tags.

Figure 5: Prompt specifically crafted to guide the model in generating interleaved image-text reasoning chains, which is consistently appended during inference.

depicted in Fig. 6. For the reward computation of answer in RL stage, as well as for benchmark evaluation, we utilize the prompt provided in Fig. 7. Finally, for inference on the REC and OVD tasks, we adopt the prompt templates shown in Fig. 8 and Fig. 9, respectively.

Prompt for CoT Completion

System Prompt

Please help me construct data that meets the specified think-answer format. Specifically, based on the given prompt, the constructed data should start with the original image and progressively focus on the regions of interest with analysis. Throughout the thinking process, you need to continuously offer the corresponding focused normalized bounding boxes with normalized depth in JSON(keep 3 decimal places of each number), describe the scene and share your thought monologue. All of these should be included within the <think> </think> tags. The final result, after comprehensive thinking, should be placed within the <answer> </answer> tags.

Directly output the constructed data, and wrap the result with 3 backticks ```. The prompt is **{prompt}**, and the final gt answer is **{response_gt}**.

Example format:

```

<think>
<area>[{"bbox_2d": [0.000, 0.000, 1.000, 1.000], "depth": 0.500}]</area>
<text>The prompt is about the color of the clothes the girl under the traffic light is wearing. I first look at the entire image and find that it is a street scene. Then I start to search for content related to the prompt in the image.</text>
<area>[{"bbox_2d": [0.500, 0.500, 0.898, 0.966], "depth": 0.345}]</area>
<text>I first notice this area, which shows some vehicles driving on the road with the depth of 0.345. Since the prompt is asking about the clothing characteristics of the girl under the traffic light, I plan to first locate the traffic light...</text>
<area>[{"bbox_2d": [0.128, 0.119, 0.490, 0.465], "depth": 0.268}]</area>
<text>Following the road, I see a traffic light on the side with the depth of 0.268...</text>
<area>[{"bbox_2d": [0.236, 0.244, 0.308, 0.312], "depth": 0.271}]</area>
<text>Further, I see a girl under the traffic light. I focus on her clothes to check the color.</text>
<area>[{"bbox_2d": [0.266, 0.274, 0.301, 0.310], "depth": 0.276}]</area>
<text>Upon closer inspection, I see that she is wearing a pink dress.</text>
</think>
<answer>
The girl under the traffic light is wearing a pink dress.
</answer>

```

Prompt

For $i = 1$ to N :

Focus on the region with the normalized bounding box with normalized depth of **{json_list_bbox_depth[i]}**, as shown by the green box in the image below. \n<image>

Figure 6: Prompt used for CoT generation, serving as the basis for constructing the SIF-50K dataset in our data generation pipeline.

Prompt for judging the answer accuracy

System Prompt

You are responsible for proofreading the answers, you need to give the score to the model's answer by referring to the standard answer, based on the given question and image.

The full score is 1 point and the minimum score is 0 points. Please directly provide the score in JSON format, for example, **{{"score": 0.8}}**, without showing the intermediate process.

The evaluation criteria require that the closer the model's answer is to the standard answer, the higher the score.

Prompt

Question: **{question}**
Standard answer: **{gt_response}**
Model's answer: **{pred_response}**

Figure 7: Prompt designed to assess the accuracy of model-generated answers against ground truth, used for computing r_{ans} and for benchmark evaluation.

Prompt Template of REC

Please provide the bounding box coordinates of the region this sentence describes: **{query}**.

Figure 8: Prompt designed for evaluating model performance on the Referring Expression Comprehension (REC) task.

Prompt Template of OVD

Please carefully check the image and detect the following objects: **{target list}**.

If there are no such targets in the image, simply respond with None.

Figure 9: Prompt designed for evaluating model performance on the Open-Vocabulary Detection (OVD) task.

More visualization

In Fig. 10, 11, 12, and 13, we present additional visualizations of *SIFThinker*. For each question-image pair, we show the depth map generated by the depth interpreter, highlight the focused regions (red bounding boxes) of *SIFThinker* during the interleaved image-text reasoning. Ground-truth annotations are also provided for comparison.

Input: What is the color of the dog?



Output:



```
<think>
<area>[{"bbox_2d": [0.0, 0.0, 1.0, 1.0], "depth": 0.616}]</area>
<text>The prompt is asking for the color of the dog. First, I look at the entire park scene. There are many
people, a statue, and bicycles. The background has greenery and a hill. Now, I need to search for a dog.</text>
<area>[{"bbox_2d": [0.502, 0.002, 0.919, 0.517], "depth": 0.758}]</area>
<text>Focusing on the right side (depth 0.758), there are trees and people. But no dog here. Let me check other
areas.</text>
<area>[{"bbox_2d": [0.228, 0.342, 0.418, 0.576], "depth": 0.766}]</area>
<text>Looking at the middle - left (depth 0.766), there's a group of people. Wait, near the bicycles, there's a
small dog. Let me zoom in.</text>
<area>[{"bbox_2d": [0.263, 0.403, 0.303, 0.475], "depth": 0.797}]</area>
<text>Focusing on the dog (depth 0.797), it's a small dog near the bicycles. Its fur color—checking the image,
it's white.</text>
</think>
<answer>
The dog is white.
</answer>
```

Ground truth: white

Figure 10: More visualization results of *SIFThinker* based on Qwen2.5-VL. We visualize the question, reasoning, ground truth, and highlight the areas of interest that the model focuses on during the reasoning process (red bounding boxes in the images).

Input: Is the color of the motorcycle red or blue?



Output:



<think>

<area>[{"bbox_2d": [0.0, 0.0, 1.0, 1.0], "depth": 0.664}]</area>

<text>The prompt asks about the color of a motorcycle. First, I look at the entire image which shows an outdoor market scene with tents, people, and a background of mountains and trees.</text>

<area>[{"bbox_2d": [0.0, 0.402, 0.248, 0.882], "depth": 0.726}]</area>

<text>Then I check the left side of the image. There's a structure with colorful fabrics, but no motorcycle visible here. So I need to scan other areas.</text>

<area>[{"bbox_2d": [0.0, 0.623, 0.052, 0.72], "depth": 0.755}]</area>

<text>Finally, focusing on the lower - left corner (bbox_2d [0.0, 0.623, 0.052, 0.72]), I see a small motorcycle. The color appears to be blue as indicated by the initial full - image view and subsequent focused check.</text>

</think>

<answer>

The motorcycle is blue.

</answer>

Ground truth: blue

Figure 11: More visualization results of *SIFThinker* based on Qwen2.5-VL. We visualize the question, reasoning, ground truth, and highlight the areas of interest that the model focuses on during the reasoning process (red bounding boxes in the images).

Input: Tell me the text on the notice board.



Output:



<think>
<area>[{"bbox_2d": [0.0, 0.0, 1.0, 1.0], "depth": 0.674}]</area>
<text>The prompt is asking for the text on the notice board. First, I look at the entire image which shows an outdoor sports field with a child holding a toy. There's a notice board in the background.</text>
<area>[{"bbox_2d": [0.554, 0.0, 0.846, 0.192], "depth": 0.838}]</area>
<text>Focusing on the upper right area (depth 0.838), there's a white sign. The text on it needs to be checked. The initial full image view shows the sign, but need to zoom in.</text>
<area>[{"bbox_2d": [0.636, 0.0, 0.756, 0.134], "depth": 0.924}]</area>
<text>Zooming in further (depth 0.924) on the sign's text. The letters "GUEST" are visible. Then, checking the next word. The full text on the sign is "GUEST TEAM".</text>
</think>
<answer>
The text on the notice board is "GUEST TEAM".
</answer>

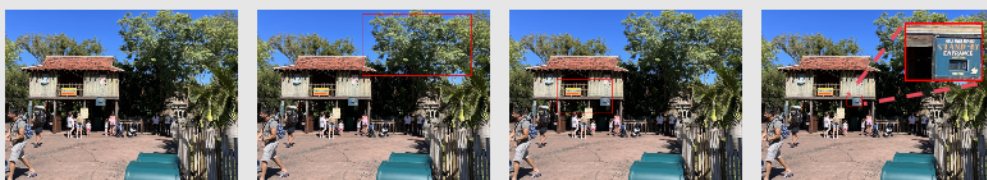
Ground truth: GUEST TEAM

Figure 12: More visualization results of *SIFThinker* based on Qwen2.5-VL. We visualize the question, reasoning, ground truth, and highlight the areas of interest that the model focuses on during the reasoning process (red bounding boxes in the images).

Input: From the information on the black framed board, how long do we have to wait in line for this attraction?



Output:



<think>

<area>[{"bbox_2d": [0.0, 0.0, 1.0, 1.0], "depth": 0.787}]</area>

<text>The prompt asks how long we have to wait in line for the attraction. First, I look at the entire scene. It's an outdoor area with a wooden building, trees, and people. There's a sign on the building that might have the answer.</text>

<area>[{"bbox_2d": [0.449, 0.027, 0.921, 0.379], "depth": 0.905}]</area>

<text>Focusing on the upper right, there are trees. But the prompt is about waiting time, so maybe the building's sign is key. Let me check the building's area.</text>

<area>[{"bbox_2d": [0.204, 0.397, 0.443, 0.597], "depth": 0.845}]</area>

<text>Now looking at the building's front. There's a yellow banner. Wait, the sign on the building—maybe that's the 'black framed board' mentioned. Let me zoom in.</text>

<area>[{"bbox_2d": [0.365, 0.489, 0.432, 0.556], "depth": 0.828}]</area>

<text>Ah, here's the sign. It says 'Wait time 10 minutes.' So the wait is 10 minutes.</text>

</think>

<answer>

The wait time for the attraction is 10 minutes.

</answer>

Ground truth: 10 minutes

Figure 13: More visualization results of *SIFThinker* based on Qwen2.5-VL. We visualize the question, reasoning, ground truth, and highlight the areas of interest that the model focuses on during the reasoning process (red bounding boxes in the images).